Absolute cross sections for the ionization-excitation of helium by electron impact

S. Bellm,[1] J. Lower,[1] E. Weigold,[1] I. Bray,[2] D. V. Fursa,[2] K. Bartschat,[3] A. L. Harris,[4] and D. H. Madison[4]
[1]*AMPL, Research School of Physical Sciences and Engineering, Australian National University, Canberra, Australian Capital Territory 0200, Australia*
[2]*ARC Centre for Antimatter-Matter Studies, Curtin University of Technology, P.O. Box U1987, Perth, Western Australia 6845, Australia*
[3]*Department of Physics and Astronomy, Drake University, Des Moines, Iowa 50311, USA*
[4]*Physics Department, Missouri University of Science and Technology, 1315 North Pine Street, Rolla, Missouri 65409, USA*
(Received 6 June 2008; published 25 September 2008)

In a recent publication we presented detailed experimental and theoretical results for the electron-impact-induced ionization of ground-state helium atoms. The purpose of that work was to refine theoretical approaches and provide further insight into the Coulomb four-body problem. Cross section ratios were presented for transitions leading to excited states, relative to those leading to the ground state, of the helium ion. We now build on that study by presenting individual relative triple-differential ionization cross sections (TDCSs) for an additional body of experimental data measured at lower values of scattered-electron energies. This has been facilitated through the development of new electron-gun optics which enables us to accurately characterize the spectrometer transmission at low energies. The experimental results are compared to calculations resulting from a number of different approaches. For ionization leading to $He^+(1s^2)^1S$, cross sections are calculated by the highly accurate convergent close-coupling (CCC) method. The CCC data are used to place the relative experimental data on to an absolute scale. TDCSs describing transitions to the excited states are calculated through three different approaches, namely, through a hybrid distorted-wave+R-matrix (close-coupling) model, through the recently developed four-body distorted-wave model, and by a first Born approximation calculation. Comparison of the first- and second-order theories with experiment allows for the accuracy of the different theoretical approaches to be assessed and gives insight into which physical aspects of the problem are most important to accurately model.

DOI: 10.1103/PhysRevA.78.032710 PACS number(s): 34.80.Dp, 34.80.Pa

I. INTRODUCTION

Studies of electron-impact-induced ionization are of importance from a number of perspectives. At the fundamental level they challenge our understanding of the many-body nature of systems of electrons whose interactions are mediated through the Coulomb potential. An improved understanding of this behavior can contribute to advances in areas such as the development of electronic devices and advanced materials by elucidating processes at the microscopic level. Second, ionization cross sections provide valuable input to simulations of atmospheric, industrial, and environmental processes. In some cases cross sections can still be more accurately measured than calculated; in other cases the reverse is true. Thus experiment can be used to both directly provide benchmark data for simulation applications and assist in the refinement of theory by providing data against which the predictions of new theoretical developments can be tested.

While recently the electron-hydrogen fully differential ionization $(e,2e)$ three-body problem has been solved to a high precision [1–4], the corresponding electron-helium ionization four-body problem has been solved to a similar accuracy only for the case where the residual electron remains in the ground state of the He^+ ion [5,6], though some aspects of a perturbative approach to the solution at high energies are not fully understood [7]. To fully characterize the electron-helium $(e,2e)$ process, fully differential cross sections should be determined for transitions to the ground and excited states of the residual ion, described by the quantum number n. However, with increasing values of n the excited-state cross sections drop dramatically in magnitude and the energy separations between successive states reduce. Consequently, high-sensitivity high-resolution electron spectrometers are required to measure these transitions. This can be achieved with time-of-flight-based technologies such as cold atom recoil ion momentum spectroscopy [8] or the reaction microscope [9], or dispersive analyzers of toroidal-sector geometry [10–13], such as employed in the present work [14]. In contrast, while the close spacing of high-n transitions poses no problem for theory since the energies are defined exactly, the calculation of small ionization cross sections poses substantial numerical challenges.

In recent publications [15,16], we presented experimental and theoretical results for the electron-impact-induced ionization of ground-state helium atoms. Cross section ratios were presented for the simultaneous ionization of the helium atom with excitation of the residual ion to the first three excited states relative to transitions leading to the $He^+(1s)$ ground state. Data were presented as ratios because they could be extracted from measurement much more accurately than the relative triple-differential cross sections (TDCSs) from which they were derived, due to cancellation of difficult-to-control experimental uncertainties. However, cross section ratios do not provide as stringent a test to theory as relative, and certainly absolute, TDCS data. In particular, the experimental ratio data do not test the absolute magnitude of calculated TDCSs and can, as we shall later see, mask problems in their shape due to fortuitous cancellation of errors.

Furthermore, in our previous work [17], absolute TDCSs for the $n=2$ and 3 excited states were reconstructed by combining experimental cross section ratios with theoretical convergent close-coupling (CCC) ground-state data. Thus their angular behavior depended on the shape of the theoretical $n=1$ CCC TDCSs through which they were normalized. In contrast, the individual, relative TDCSs presented here are directly measured, hence circumventing these limitations and providing direct experimental tests to theory. This has been achieved through the development of new low-energy electron-deceleration optics for our electron gun, enabling us to much more reliably implement the systematic procedure, described in [14], to correct for nonuniformities in detector gain and analyzer transmission at low values of scattered electron energy.

Finally, the present measurements are performed at considerably lower values of average energy for the slow ejected electron (20 eV compared to 44 eV) compared to our earlier work [15,16], allowing us to more stringently test various theoretical approaches by extending the kinematic range over which they can be tested. The present TDCS experimental data are placed on an absolute scale by normalizing them to the CCC calculations, which have been checked to yield the correct total, single-, and double-differential ionization cross sections for the kinematics of interest.

II. APPARATUS AND EXPERIMENTAL TECHNIQUES

The apparatus has been extensively described in a previous publication [14], hence only a short account is provided here. A beam of spin-polarized electrons is formed through extracting, by means of a weak electric field, photoelectrons released from a strained gallium-arsenide photocathode illuminated by monochromatic 850 nm circularly polarized laser light. Following extraction, the beam is deflected through 90°, accelerated to 600 eV, and transported through a differentially pumped vacuum chamber before entering the collision chamber in which the analyzers are housed.

In the collision chamber a seven-element electrostatic lens is employed to decelerate the electron beam to the chosen experimental collision energy E_0 and focus it on to the helium target beam. The overlap of electron and helium beams defines a localized interaction volume. The helium beam is formed by effusion through a 1 mm internal-diameter molybdenum needle with the electron beam passing 1 mm above its orifice. As no significant spin-dependent effects are expected in the scattering of electrons from low-Z targets, data are presented here for an ensemble of unpolarized projectile electrons. This was obtained by illuminating the photocathode alternately with laser light of right-circular and left-circular polarization for equal measurement times.

The seven-element deceleration lens, designed using SIMION simulation software [18], replaces the five-element lens [14] used for previous measurements. In contrast to its predecessor, deceleration is performed in two steps, rather than one, thereby enabling well-focused electron beams to be created at lower values of impact energies. As a result, calibration of the ejected-electron analyzer could be performed at lower energy values than previously, with elastic scattering of electrons from the helium target being used for that purpose. The absolute energy scale of the primary electron beam was established by measuring the well-known helium $1s2s^2\ ^2S$ negative-ion resonance at 19.37 eV impact energy.

Scattered electrons are momentum analyzed in one of two toroidal-sector electrostatic electron energy analyzers located on opposite sides of the incident beam. Measurements were performed in coplanar scattering geometry, implying only $(e,2e)$ electron pairs emitted within a plane containing the primary electron beam are detected. Terminating each analyzer is a pair of micro-channel-plate electron multipliers followed by a crossed delay-line detector [8] used to determine the spatial and temporal coordinates (x_i,y_i,t_i) for electrons arriving at each analyzer exit plane. From these coordinates, $(e,2e)$ electron pairs are identified and electron momenta are deduced.

One analyzer measures electrons over the angular range $20° \leqslant \theta_1 \leqslant 60°$ and the other over the range $20° \leqslant \theta_2 \leqslant 120°$. Due to the limited size of the detectors (80 mm diameter) only a 40° degree band of emission angles can be measured in each analyzer at a given time. For the analyzer of smaller angular acceptance, the detector is fixed to encompass the angular range $20° \leqslant \theta_1 \leqslant 60°$. For the other analyzer the detector is movable, enabling the mean angle of the detection range to be varied from 40° to 100°. For the present experiment, successive measurements were performed at mean detection angles of 40, 70, and 100° to cover the full range of emission angles $20° \leqslant \theta_2 \leqslant 120°$. Sufficient angular overlap (10°) of the three acceptance ranges enabled cross normalization of data accumulated for the three positions to be accurately performed.

The experiment was performed for asymmetric energy sharing between the two final-state electrons comprising each $(e,2e)$ electron pair. The average measured energies for the fast (scattered) and slow (ejected) electrons, E_1 and E_2, were 150 and 20 eV, respectively. In contrast to our previous work [15,16], considerably lower values for ejected-electron energies were chosen to extend the kinematic range over which we could test theory. As before, the ejected-electron energy-acceptance band was carefully chosen to encompass a region without resonance contributions, whose presence complicates theoretical calculations. The average energy of the measured fast scattered electron was chosen to be sufficiently high to justify, at least to some extent, a perturbative treatment, but low enough to ensure that count rates would be sufficient to render measurement of weak transitions to the $n=2,3$ excited ion states feasible. Consistent with energy conservation, the collision energy E_0 was adjusted, respectively, to 196, 235.4, and 243.0 eV for transitions to the $n=1$, 2, and 3 states of the helium ion. To average over any long-term instrumental drifts, these three collision energies were stepped through many times an hour, with 40% of data collection time spent on each of the two excited-state transitions and the remaining 20% on the $n=1$ transition.

The energy-acceptance windows for both analyzers was 10 eV. For the fast-electron analyzer, electrons were measured over the energy band $145 \leqslant E_1 \leqslant 155$ eV and for the slow-electron analyzer $15 \leqslant E_2 \leqslant 25$ eV. Within each window, electron energies were determined to within around 0.60 eV. Combined with an energy spread of 0.20 eV for the

primary beam, a 0.65 eV binding-energy resolution was achieved.

To ensure an accurate experimental cross normalization between data for $n=1$, 2, and 3 transitions by minimizing energy-dependent changes to the interaction-volume geometry (upon which the analyzers' transmission is weakly dependent), the beam deceleration optics was adjusted as the incident energy was changed. Additionally, the beam current was measured in a Faraday cup positioned behind the interaction region and continuously recorded. This enabled relative cross sections to be corrected for any changes in electron-beam current as the collision energy was stepped through.

III. THEORETICAL TREATMENTS

The ionization-excitation of helium is a highly correlated process in which two atomic electrons change their quantum state. To accurately predict transition strengths requires an accurate description both of the initial-state wave function and of the interactions inherent to the collision. To date, none of the fully nonperturbative approaches such as CCC, exterior complex scaling [1], or time-dependent close coupling [19] has been applied to calculate fully differential ionization cross sections involving transitions to the He^+ excited states. While there is no fundamental reason why these methods could not be applied, such an implementation is by no means straightforward. Indeed, in the case of the CCC method, the current diagonalization approach to the generation of the target states would need major modification. While such an extension is presently under consideration, it remains a longer-term goal. Currently, therefore, perturbative approaches remain the only available means to describe the problem.

A number of calculations are presented here, with the experimental data used to test the relative merits of different approximation schemes, to assess the relative importance of neglecting or including different physical aspects of the problem, and to establish which areas provide the greatest potential for future improvement. As will be shown below, the predictions depend strongly on the order of calculation and on the choice and quality of approximations they incorporate. A detailed review of previous theoretical and experimental studies in this area was presented in our previous publication [16] and is therefore not repeated here.

The simplest calculation presented is a first-Born-approximation (FBA) calculation in which the fast electron is treated as a plane wave in both the initial and final states while the slow ejected electron is treated using a distorted wave. The $\boldsymbol{T}$ matrix for this model is given by

$$T_{fi} = \langle \beta_f(\boldsymbol{r}_1)\psi_f^{(-)}(\boldsymbol{r}_2)\psi_{nlm}(\boldsymbol{r}_3)|V_i|\beta_i(\boldsymbol{r}_1)\psi_i(\boldsymbol{r}_2,\boldsymbol{r}_3)\rangle \qquad (1)$$

with

$$V_i = -\frac{2}{\boldsymbol{r}_1} + \frac{1}{|\boldsymbol{r}_1-\boldsymbol{r}_2|} + \frac{1}{|\boldsymbol{r}_1-\boldsymbol{r}_3|}, \qquad (2)$$

where $\boldsymbol{r}_1$ is the projectile coordinate while $\boldsymbol{r}_2$ and $\boldsymbol{r}_3$ are the coordinates of the atomic electrons. Furthermore, $\beta_{i,f}(\boldsymbol{r}_1)$ is the plane wave representing the initial- or final-state wave function of the fast electron, $\psi_f^{(-)}(\boldsymbol{r}_2)$ is the distorted wave for the slow electron, $\psi_{nlm}(\boldsymbol{r}_3)$ is the hydrogenic final state of He^+, and $\psi_i(\boldsymbol{r}_2,\boldsymbol{r}_3)$ is the initial bound-state wave function for helium. The integration over the projectile electron is performed analytically using the Bethe integral, and the remaining integrations over the two atomic electrons are performed numerically.

Results from a much more elaborate four-body distorted wave (4DW) calculation [20] are also presented. In this model, all particles in the continuum are described by distorted waves, and the Coulomb interaction between the two outgoing electrons is included exactly. The $\boldsymbol{T}$ matrix for this model is given by

$$T_{fi} = \langle \chi_f(\boldsymbol{r}_1)\psi_f^{(-)}(\boldsymbol{r}_2)\psi_{nlm}(\boldsymbol{r}_3) \times C(\boldsymbol{k}_{12},\boldsymbol{r}_{12})|V_i - U_i|\chi_i(\boldsymbol{r}_1)\psi_i(\boldsymbol{r}_2,\boldsymbol{r}_3)\rangle, \qquad (3)$$

with V_i given by (2). Here $\chi_{i,f}(\boldsymbol{r}_1)$ is the distorted wave for the initial or final state of the "fast" electron and U_i is the spherically symmetric distorting potential used to calculate $\chi_i(\boldsymbol{r}_1)$. Therefore, the term $V_i - U_i$ in (3) represents the nonspherical part of the initial-state projectile-atom interaction. Finally, $C(\boldsymbol{k}_{12},\boldsymbol{r}_{12})$ is the Coulomb distortion factor that accounts for the electron-electron interaction between the two continuum electrons in the final state. This term is often referred to as the C factor or postcollision interaction (PCI); it depends on the coordinates and relative momenta of the two outgoing electrons. By treating the projectile interactions, in both the initial and the final state, through distorted waves and explicitly including PCI, the 4DW model includes all projectile interactions and hence is an asymptotically exact solution to the Schrödinger equation [21,22]. Thus, in addition to containing all the physics contained in the FBA, the 4DW additionally includes the projectile-target interaction and an accurate representation of PCI. For both FBA and 4DW calculations, a highly accurate 20-term Hylleraas wave function, including both radial and angular correlations, was employed to describe the ground-state helium wave function [23]. For ionization-excitation calculations, where the interaction between the projectile electron and the two atomic electrons is treated to first order, the accuracy of the helium bound-state wave function is crucial, as in the absence of initial-state correlation and shake-off, the first-Born term is identically zero. As a consequence, contributions from processes involving second-order interactions between the projectile and atomic electrons are expected to play a significant role in determining TDCSs for the ionization-excitation process.

A third set of calculations were performed using the hybrid distorted-wave+R-matrix (close-coupling) (DWRM) method. In this method, the interaction of a fast electron with the target is treated perturbatively, while the initial bound state and the e-He^+ collision of a slow ejected electron and the residual ion is treated via a convergent R matrix with pseudostates (close-coupling) expansion. While not as accurate as the Hylleraas wave function employed for the FBA and 4DW calculations, an accurate multiconfiguration expansion wave function of energy −2.902 332 0 a. u. was used to

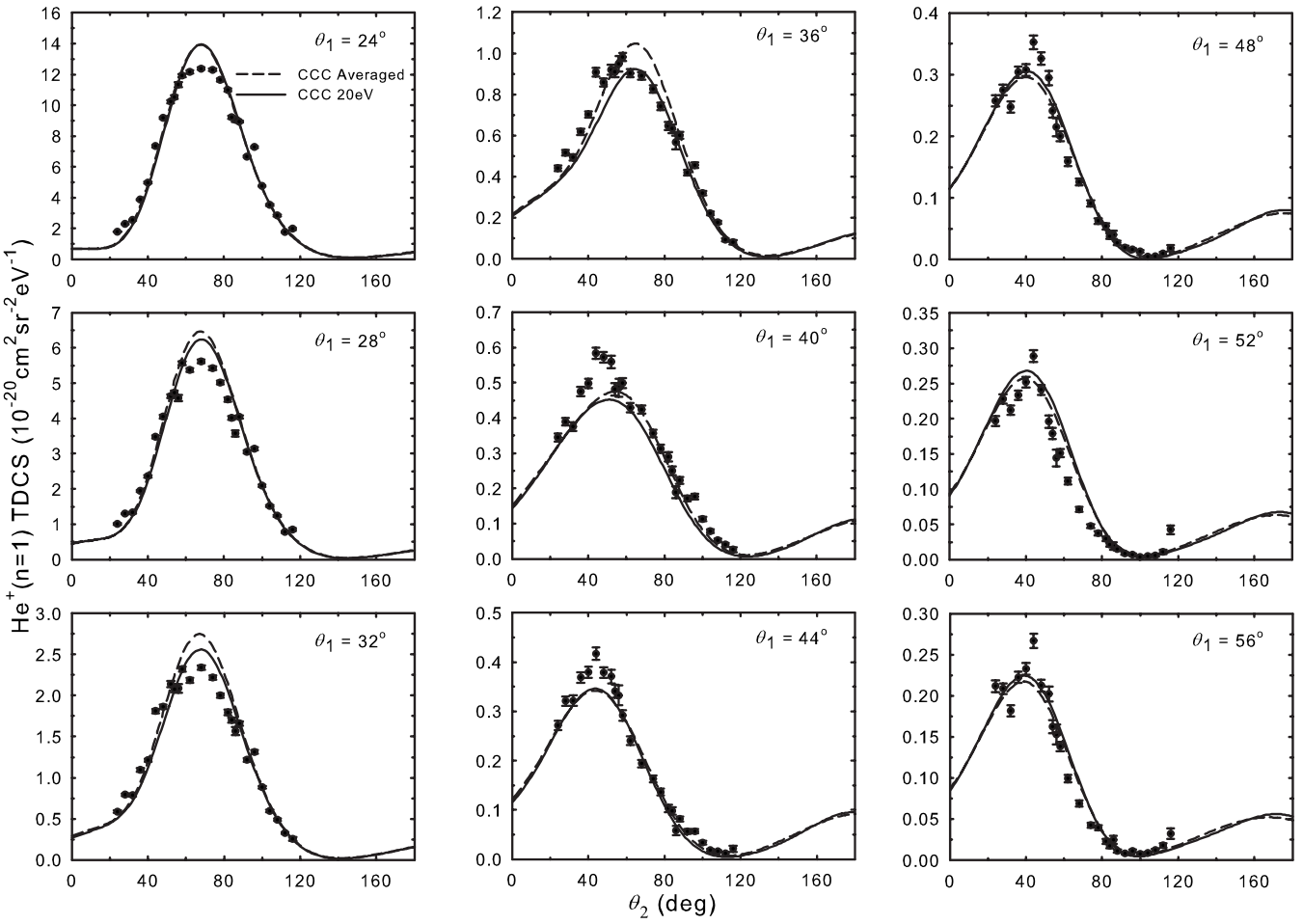

FIG. 1. Experimentally derived and theoretical TDCSs for ionization of He($1s^2$) leading to ground-state $He^+(1s)$. The primary energy E_0 is 194.6 eV and the two final-state electrons have average energies of 150 and 20 eV, respectively. The solid lines are results of CCC calculations performed for the specific values of scattering angles θ_1 and θ_2 indicated in each frame. The dashed lines correspond to an average of CCC calculations taking into account the finite angular and energy resolution of the experiment (see text for details). The relative experimental results have been normalized to this average for the best overall visual fit using a single normalization constant.

describe the helium ground state. (For details and further references, see Bellm *et al.* [15,16].) These calculations were performed in two variants, labeled DW1-RM and DW2-RM, in which the projectile-target interaction was treated to first and second order, respectively. We note that the DW1-RM, DW2-RM, FBA, and 4DW calculations all neglect exchange. However, under the present highly asymmetric energy-sharing kinematics, exchange contributions are expected to be small.

When comparing the DW2-RM with the 4DW calculations, the following similarities and differences between the two approaches should be noted. (1) Both approaches use distorted waves for the initial projectile wave function. (2) The 4DW method uses a slightly better (regarding the total energy) initial-state wave function for He. (3) Both approaches use a distorted wave for the final state of the projectile. (4) The DW2-RM approach uses a better wave function for the ejected electron. (5) The DW2-RM method accounts for second-order collisions between the projectile and target while the 4DW method includes only first-order collisions. (6) The 4DW calculation contains, to infinite order, final-state electron-electron interactions (PCI), which are neglected in the DW2-RM method.

Finally, calculations were performed using the CCC model. While all of the above calculations were applied to describe excitation to both the ground and excited states of the helium ion, application of the CCC method was restricted to determining the TDCS for ionization leading to the $He^+(1s)$ state and to normalizing the experimental data. Based on previous experience for transitions to the He^+ ground state [5,6,24], we expect the CCC results to be accurate for all kinematics and geometries. In CCC, ionization is associated with excitation of positive-energy pseudostates, which are obtained by diagonalizing the target Hamiltonian in a Laguerre basis of size N_l. The frozen-core approximation, where one of the electrons is described by the $1s$ orbital of He^+, is used. This reduces the four-body problem to effectively a three-body one, making convergence studies much easier. The close-coupling equations are solved in momentum space with the excitation amplitudes for the positive-energy states used directly to determine all of the cross sections [5]. Here, we took $N_l=40-l$ with $l \leqslant l_{\max}=5$. Exchange

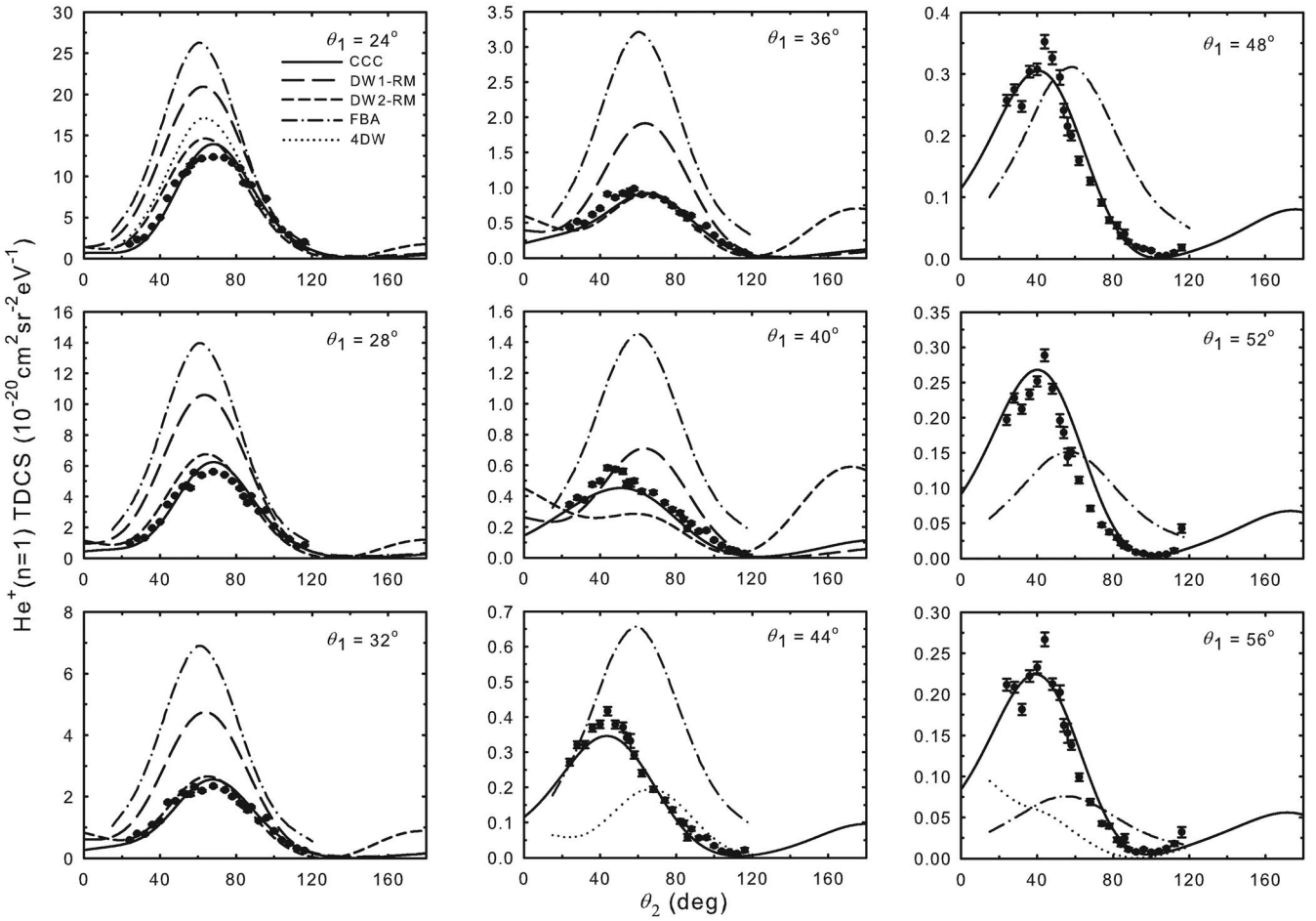

FIG. 2. Same experimental data and CCC calculations (solid line) as in Fig. 1 compared to a first-order Born approximation (FBA) calculation (dotted-dashed line), the 4DW calculation (dotted line), and first- and second-order calculations using the hybrid distorted-wave+R-matrix method [DW1-RM (long-dashed line) and DW2-RM (short-dashed line), respectively].

is included, ensuring that correct total, single-, and double-differential cross sections are in absolute agreement with available experiment [25]. This gives us confidence that the CCC-calculated fully differential cross sections are also accurate in both shape and magnitude. For this reason they are used to normalize the present experiment.

IV. RESULTS AND DISCUSSION

Figure 1 shows the experimental TDCSs compared to results of CCC calculations for transitions to the $He^+(n=1)$ ground state. The solid lines correspond to calculations performed for $E_2=20$ eV and for the specific values of θ_1 and θ_2 indicated in each frame. The dashed lines are the result of averaging CCC calculations over the 10 eV analyzer energy-acceptance windows and over the 4° angular intervals into which both θ_1 and θ_2 data are binned. The experimental data are normalized to the average cross section for best visual fit, the same normalization constant being used across the whole range of θ_1.

First, in terms of predicting the shape of the respective angular distributions (θ_2 dependence), the averaged theory is generally very successful, although some small discrepancies are evident. Particularly impressive is its ability to predict the dependence of cross section on θ_1, the cross section being reduced by around a factor of 50 as θ_1 is increased from 24 to 56°.

Second, comparison of the two calculations shows the effect of the rather broad instrumental angular and energy resolution to be small. This is comforting for the following reason. Although we can resolve energy values E_1 and E_2 to better than 0.4 eV and emission angles θ_1 and θ_2 to better than 2°, presenting data for smaller volumes of momentum phase space would result in significantly diminished statistics in the data plots. While not a problem for the $n=1$ transition data, this would be highly problematic for the $n=3$ transition, as the associated cross sections are typically three orders of magnitude smaller (see Fig. 4 below). Thus we present our experimental data with a lower resolution (10 eV acceptance windows, 4° bin size) for comparison with theory.

Figure 2 shows the same experimental data and CCC calculation of Fig. 1, employing the same normalization procedure, compared to the other three sets of calculations. In light of the relative insensitivity to averaging for the $n=1$ calculations, we compare nonaveraged calculations for the excited states directly to the experimental data to limit computational

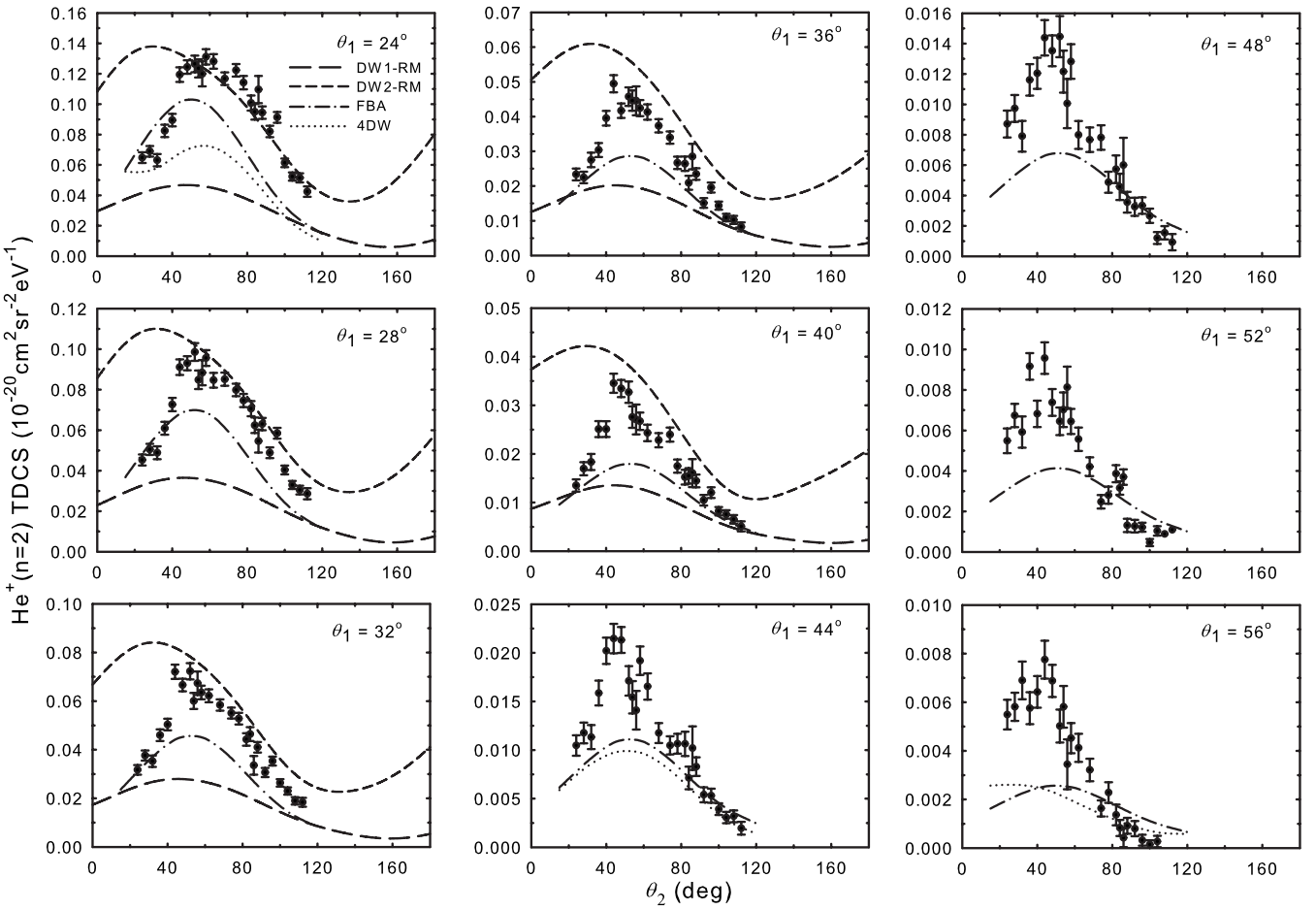

FIG. 3. TDCSs for transitions leading to the $He^+(n=2)$ states. The primary energy E_0 is 235.4 eV and the two final-state electrons have average energies of 150 and 20 eV, respectively. The experimental data are put on an absolute scale using the results of CCC calculations for the $n=1$ transition (see text for details). No CCC calculations are presented for transitions to $He^+(n=2)$; the other calculations and the legend are as in Fig. 2.

demands. The calculation labeled FBA (dotted-dashed line) is a first-order Born approximation calculation, the 4DW calculation is represented by the dotted line, and the calculations labeled DW1-RM (long-dashed line) and DW2-RM (short-dashed line) are, respectively, first- and second-order calculations using the hybrid distorted-text+R-matrix (close-coupling) method.

As expected for the $n=1$ transition, the CCC calculation performs the best of all calculations. For scattering angles $\theta_1 \leqslant 36°$, the second-order DW2-RM calculation performs well. However, the width of the binary peak is slightly overestimated at smaller angles and a small angular shift to lower scattering angles θ_2 is evident between the predicted and measured positions of the peak maximum. In comparison, the DW1-RM calculation severely overestimates the TDCSs and again does not accurately predict the peak position of the cross section maximum. Comparison of these two calculations with experiment suggests that second-order effects are very important to get the magnitude correct, even for this case of ionization without excitation, where only one bound electron changes its quantum number. At larger values of θ_1 the DW1-RM and DW2-RM calculations both diverge strongly from measurement. The discrepancy between experiment and theory at 40° reflects this trend. This behavior may be due to the neglect of the exchange amplitude in the model, which was designed for strongly asymmetric energy sharing and small scattering angles. It is not trivial to improve the theory toward the more general case. Work in this direction is currently in progress. For the above reasons, hybrid results are presented here only for fast-electron detection angles up to 40°.

The FBA strongly overestimates the cross sections at small values of θ_1 and underestimates it at larger θ_1 values. The predicted position of the cross section maximum is seen to deviate strongly from measurement as θ_1 is increased. The 4DW calculation is presented only at selected values of scattering angle θ_1 (24, 44, and 56°) due to its computationally intensive nature. This calculation, which in contrast to the FBA employs a distorted wave for the fast electron and includes PCI, provides a much better description of the experimental data at $\theta_1 = 24°$. At 44 and 56°, on the other hand, the 4DW calculation shows a poorer shape description of the experimental data than the FBA and, at 44° in particular, a dramatically smaller prediction for the TDCS magnitude. Large differences between the predictions of these two models suggest that an accurate treatment of the projectile-target

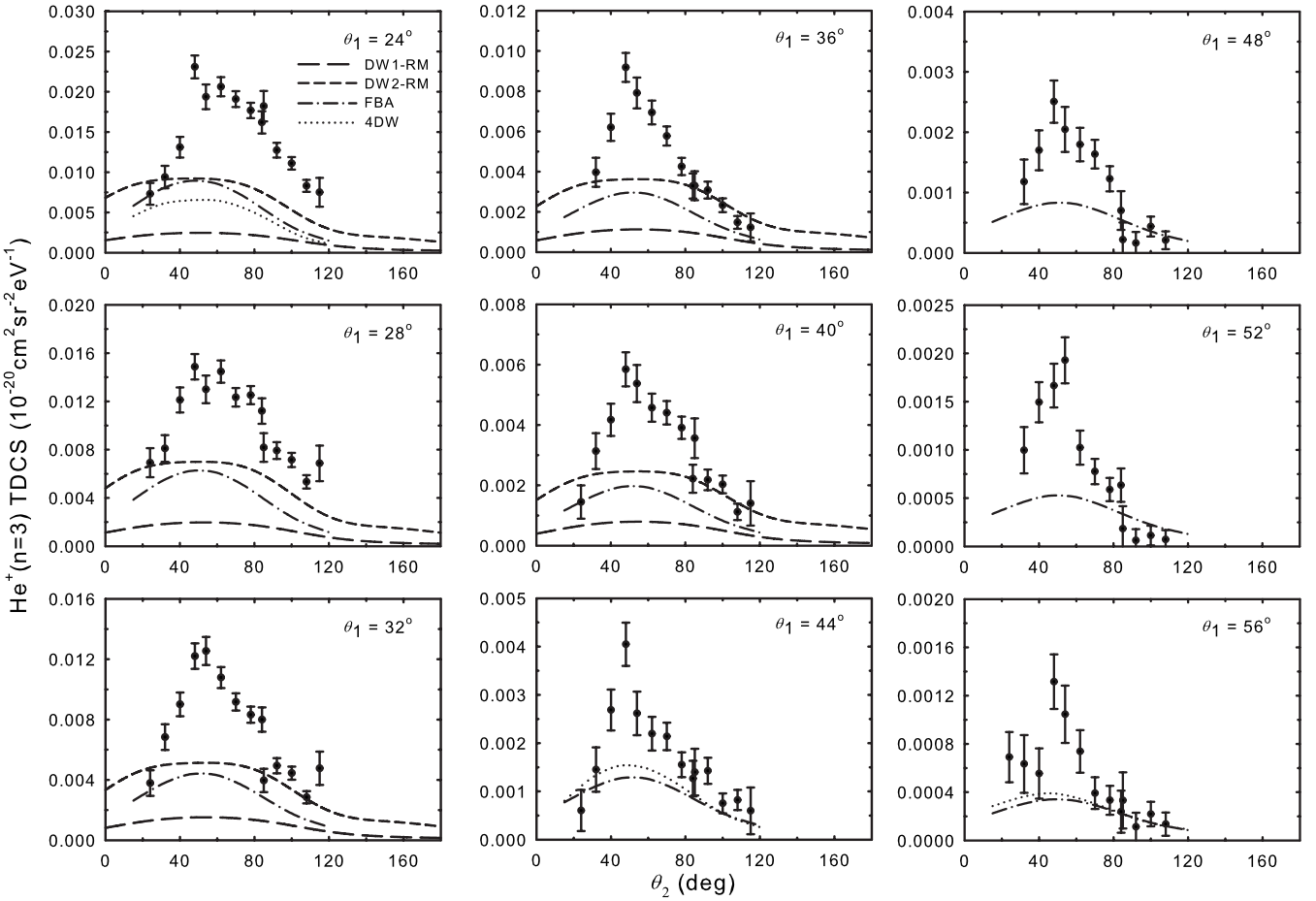

FIG. 4. TDCSs for transitions leading to the $He^+(n=3)$ states. The primary energy E_0 is 243.0 eV and the two final-state electrons have average energies of 150 and 20 eV, respectively. The legend and the normalization procedure for the experimental data are as described in the Fig. 3 caption.

interaction and PCI may be very important for this transition under the present kinematics. The fact that the 4DW does so poorly for large scattering angles suggests that higher-order perturbation terms are very important for close collisions.

Figures 3 and 4, respectively, exhibit TDCSs for transitions leading to the $He^+(n=2)$ and $He^+(n=3)$ states. The single normalization constant adopted in Fig. 1, in which the experimental ground-state TDCS data are normalized to CCC theory, puts the $n=2$ and 3 data on an absolute scale. This is because our experimental method inherently determines the relative strengths for the $n=1$, 2, and 3 transitions.

Figure 3 compares the DW1-RM, DW2-RM, 4DW, and FBA calculations to the $n=2$ experimental data. Overall the second-order DW2-RM hybrid calculation provides the best description. At large values of θ_2 it predicts magnitudes for the TDSCs quite accurately, although it fails to describe their rapid fall-off at smaller values of θ_2. The first-order DW1-RM hybrid calculation performs significantly worse, underestimating the cross section magnitudes at all values of θ_1. Large differences between the magnitudes of the DW1-RM and DW2-RM results (larger than for the $n=1$ case) show that inclusion of second-order effects is essential to correctly predict TDCS magnitudes for the highly correlated ionization-excitation process.

Interestingly, in sharp contrast to the $n=1$ case, the FBA predictions for the $n=2$ transition are closer to the experimental values than those of the DW1-RM calculation. Not only does the FBA provide a better estimate of the magnitude of the cross section maximum, but also provides a better shape description of the experimental data than either the DW1-RM or DW2-RM calculations, in particular, predicting the rapid decrease in TDCS magnitude for smaller values of θ_2. This may simply be the result of a fortuitous cancellation of effects resulting from shortcomings in the FBA model. As seen from the $n=1$ case, and also known from many other cases, the FBA tends to overestimate the cross section for direct processes near their maxima. Furthermore, as illustrated by the comparison of DW1-RM and DW2-RM calculations above, ionization-excitation at the kinematics of the current investigation is strongly influenced by second-order, and presumably even higher-order, processes. Hence first-order theories will tend to underestimate the cross sections for such cases. As a result, the FBA cannot reliably predict the cross section ratio of ionization without excitation to ionization with excitation. On the other hand, initial-state correlations are also expected to be very important for ionization-excitation, and thus the superior shape representation provided by the FBA relative to the DW1-RM and DW2-RM

calculation may, to some degree, reflect the more accurate representation of the helium ground state provided by the Hylleraas wave function.

Also of interest is that, in spite of its greater sophistication, the 4DW calculation provides a poorer description of the experimental data compared to the FBA calculation at $\theta_1=24°$ and similar predictions at $\theta_1=44$ and 56°. At all three θ_1 angles it underestimates the experimental data by a factor of about 2 and predicts a smoother angular behavior than is observed experimentally. This again illustrates that inclusion of more physics in an approximate model does not necessarily improve the overall results. Also noteworthy is the fact that the differences in predictions of the FBA and 4DW models are much smaller for this case of ionization-excitation than are evident in Fig. 2 for ionization without excitation. The differences between the FBA and 4DW calculations are projectile-target and projectile–ejected-electron interactions. These results show that these interactions are less important for ionization-excitation than for single ionization. In fact, for the 44 and 56° cases, these interactions have almost no effect at all.

Figure 4 shows TDCSs for transitions leading to the $He^+(n=3)$ states. We note that the cross sections for these transitions are around a factor of 500 smaller than for the $n=1$ case, thus presenting a severe challenge to both experiment and computation. In this case all calculations severely underestimate the experimental cross sections, typically by a factor of 2–10 at the peak maximum. Once again, the second-order DW2-RM method performs the best of all calculations in predicting the magnitude of the TDCSs, although its predictions are not substantially different from those of the first-order FBA calculation. As before, it seems likely that cancellation of errors makes the FBA look much better than might be expected in light of the limited amount of physics accounted for in this model. For this excited state the DW2-RM calculations predict flatter angular distributions than are observed experimentally, with the FBA again providing a superior description of the TDCS shape. As for the $n=2$ case, we again observe only small differences in the predictions of the 4DW and FBA models, in contrast to the $n=1$ behavior for the same scattering angles.

It is intriguing that the FBA actually does the best job of predicting the shape and peak positions of the data. This may be completely fortuitous. However, what the FBA has is the best possible treatment of initial-state correlation between the two bound electrons, which is expected to play an important role for ionization-excitation. One possible explanation for these results is that initial-state correlation plays a crucial role in determining the shape of the TDCS and second- and higher-order effects determine the magnitude. For these kinematics, PCI is relatively unimportant, as also are projectile-target interactions.

For completeness, we finish by presenting in Figs. 5 and 6 the cross section ratios for the $n=1$ to $n=2$ and $n=1$ to $n=3$ transitions, respectively. The experimental data they present are of superior statistical quality than would result from directly using the data presented in Figs. 1–4. This is because, unlike in the extraction of TDCS data, we do not need to first correct for energy or angular variations in detector efficiency or analyzer transmission to extract this quantity, as such uncertainties cancel out in the quotient. This improves the accuracy of the ratio as the correction procedure introduces additional statistical fluctuations into the individual extracted TDCSs. As would be expected from the individual TDCS data of Figs. 1–4 and up to 40° where it stops, the DW2-RM calculation is closest to the experimental results, with the other calculations all greatly overestimating the experimentally derived values at the smaller values of θ_1. For $\theta_1=24°$, the FBA and the 4DW calculations yield very similar results. At the larger angles the two calculations are seen to diverge from one another, with the 4DW calculation providing a substantially improved description of the data at $\theta_1=44°$ and some improvement at $\theta_1=56°$. However, this is obviously fortuitous since the 4DW $n=1$ TDCS does not agree with experiment for large scattering angles.

V. CONCLUSIONS

We have presented a body of experimental benchmark data for the electron-impact-induced ionization of ground-state helium atoms leading to He^+ ions left in their ground and excited states. Measurements were performed at primary-electron energies E_0 of 194.6, 235.4, and 243.0 eV for transitions leading to the $n=1$, 2, and 3 states, respectively. The two final-state electrons were measured at average energies of 150 and 20 eV. Facilitated through the development of new electron gun optics and in contrast to our previous experimental work [15,16], individual TDCS data are now presented and the measurements are extended to much lower values of scattered electron energies. The experimental data are compared to a variety of first- and second-order calculations of differing levels of sophistication and computational intensiveness, as well as to the highly accurate CCC method, which was used to place the experimental data on an absolute scale.

For transitions leading to the ground ionic state, the CCC method reproduced the experimental data to high accuracy and, as expected, was superior to the first- and second-order theories which, except for the DW2-RM hybrid method at scattering angles below ≈36°, were unable to accurately predict the angular variations of the TDCSs. We suspect that the presence of unknown and thus unaccounted-for systematic errors in the experiment, rather than deficiencies in theory, largely account for the small residual discrepancies between the CCC predictions and experiment. Large differences were observed between the first- and second-order models, showing the importance of including second-order (and possibly higher-order) effects to accurately describe the data. Furthermore, large differences were observed between the 4DW and FBA first-order theories, respectively with and without the inclusion of PCI and a distorted wave treatment of the fast electron, suggesting that the description of both these effects is also important for this transition at the present kinematics.

For transitions leading to the $n=2$ and 3 excited states, a theoretically more challenging problem to treat, both first- and second-order theories have great difficulties in describing the angular behavior and magnitudes of the normalized

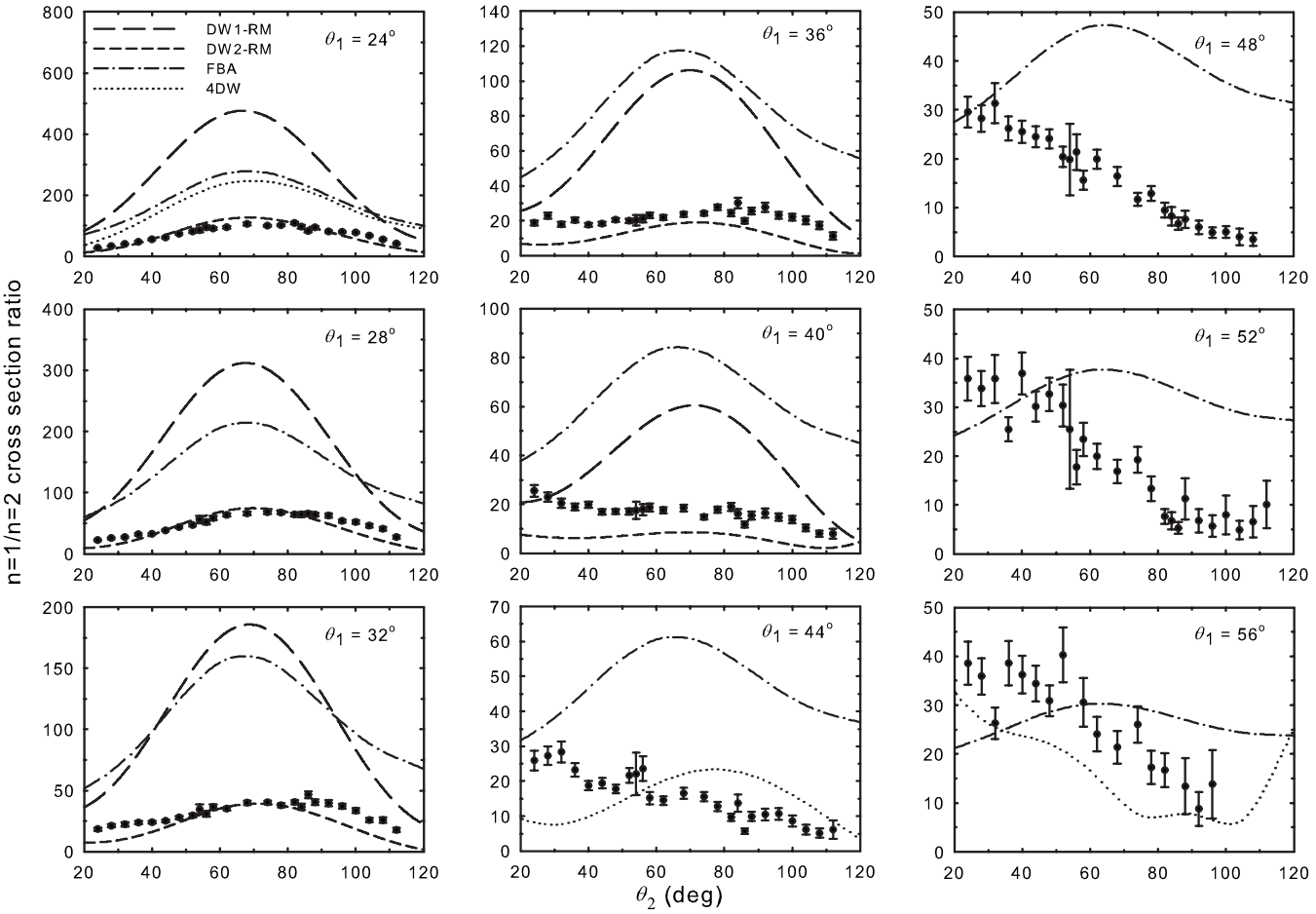

FIG. 5. TDCSs for ionization of He($1s^2$) leading to $He^+(n=1)$ divided by the corresponding TDCSs for leaving the He^+ ion in the $n=2$ states. The primary energy E_0 is 194.6 eV for the $n=1$ states and 235.4 eV for the $n=2$ states, with the two final-state electrons having average energies of 150 and 20 eV, respectively. The legend is as in Fig. 2.

experimental TDCSs. Up to scattering angles $\theta_1 < 40°$, the hybrid second-order theory gives the best description of the experimental TDCSs, although severely overestimating their magnitudes at small values of θ_2 for the $n=2$ transition. For the $n=3$ transitions, all theories grossly underestimate the experimental data, in particular their angular maxima, by more than a factor of 2. Interestingly, the differences between the 4DW and FBA calculations appear much smaller for the case of ionization-excitation than for transitions to the $n=1$ ion state, which indicates that the projectile-target and projectile-electron interactions are less important for excitation-ionization than for single ionization.

The discrepancy between the 4DW model and experiment is partly attributable to the large scattering angles involved. Previous work with the three-body distorted wave model showed that the theory agreed nicely with the shape and magnitude of absolute experimental data for small projectile scattering angles. However, as the scattering angle increased, the shape agreement remained good, while the magnitude became incorrect [26]. It is possible that for excitation-ionization the exchange amplitude (neglected in the present calculation) may not be small enough to be neglected. An additional source of discrepancy could be the distorted wave treatment of the ejected electron. Replacement of the distorted wave with a close-coupling treatment for the ejected electron might improve agreement with experiment. However, for ejected-electron energies above 10 eV, it is not expected that this would have a significant effect on the results. Further theoretical and experimental developments are therefore required to resolve the outstanding discrepancies in this area.

On the experimental front, the present spectrometer is being modified to include new deceleration lenses of improved design for the scattered electron analyzers. This modification promises higher data rates at improved energy resolution and decreased sensitivity of TDCS measurements to stray fields or inaccuracies in mechanical alignment. Furthermore, binning methods are being developed in which the detector on the larger analyzer will be continuously scanned through the full angular range of θ_2, thereby enabling data collected at specific values of θ_2 to be averaged over all positions on the detector. As a result of these changes, the already small systematic errors present should be further reduced and an analysis of the weak excited-state transitions up to and including $n=5$ should be possible. The result will be the provision of even more stringent tests for theory in the near future.

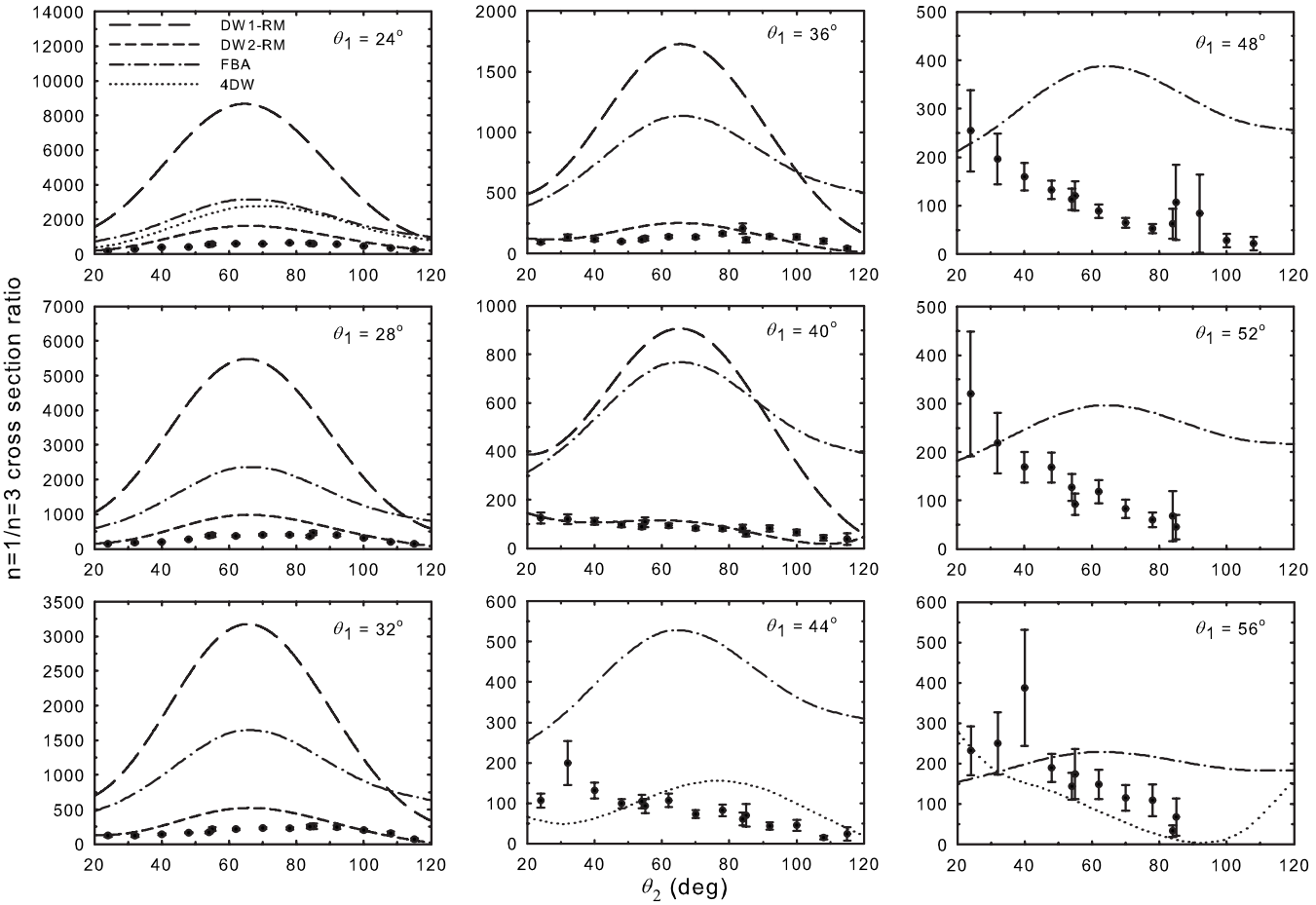

FIG. 6. TDCSs for ionization of He($1s^2$) leading to $He^+(n=1)$ divided by the corresponding TDCSs for leaving the He^+ ion in the $n=3$ states. The primary energy E_0 is 194.6 eV for the $n=1$ states and 243.0 eV for the $n=3$ states, with the two final-state electrons having average energies of 150 and 20 eV, respectively. The legend is as in Fig. 2.

ACKNOWLEDGMENTS

We gratefully acknowledge the assistance of the Australian Research Council under Grant No. DP0452553 (S.B. and J.L.) and the United States National Science Foundation under Grants No. PHY-0757755 (K.B.) and No. PHY-0757749 (A.L.H. and D.H.M.). A.L.H. and D.H.M. would also like to acknowledge the use of Los Alamos National Laboratory Institutional Computing Resources, as well as support by the National Science Foundation through TeraGrid resources provided by the Texas Advanced Computing Center.

[1] T. N. Rescigno, M. Baertschy, W. A. Isaacs, and C. W. McCurdy, Science **286**, 2474 (1999).
[2] J. Colgan, M. S. Pindzola, F. J. Robicheaux, D. C. Griffin, and M. Baertschy, Phys. Rev. A **65**, 042721 (2002).
[3] I. Bray, D. V. Fursa, A. Kheifets, and A. T. Stelbovics, J. Phys. B **35**, R117 (2002).
[4] I. Bray, Phys. Rev. Lett. **89**, 273201 (2002).
[5] I. Bray and D. V. Fursa, Phys. Rev. A **54**, 2991 (1996).
[6] A. T. Stelbovics, I. Bray, D. V. Fursa, and K. Bartschat, Phys. Rev. A **71**, 052716 (2005).
[7] M. Schulz, R. Moshammer, D. Fischer, H. Kollmus, D. H. Madison, S. Jones, and J. Ullrich, Nature (London) **422**, 48 (2003).
[8] R. Dörner, V. Mergel, O. Jagutzki, L. Spielberger, J. Ullrich, R. Moshammer, and H. Schmidt-Böcking, Phys. Rep. **330**, 95 (2000).
[9] J. Ullrich, R. Moshammer, A. Dorn, R. Dörner, L. Ph. H. Schmidt, and H. Schmidt-Böcking, Rep. Prog. Phys. **66**, 1463 (2003).
[10] A. Duguet, A. Lahmam-Bennani, M. Lecas, and B. El Marji, Rev. Sci. Instrum. **69**, 3524 (1998).
[11] T. J. Reddish, G. Richmond, G. W. Bagley, J. P. Whightman, and S. Cvejanović, Rev. Sci. Instrum. **68**, 2685 (1997).
[12] M. Takahashi, T. Saito, M. Matsuo, and Y. Udagawa, Rev. Sci. Instrum. **73**, 2242 (2002).
[13] R. W. van Boeyen and J. F. Williams, Rev. Sci. Instrum. **76**,

063303 (2005).
[14] J. Lower *et al.*, Rev. Sci. Instrum. **78**, 111301 (2007).
[15] S. Bellm, J. Lower, and K. Bartschat, Phys. Rev. Lett. **96**, 223201 (2006).
[16] S. Bellm, J. Lower, K. Bartschat, X. Guan, D. Weflen, M. Foster, A. L. Harris, and D. H. Madison, Phys. Rev. A **75**, 042704 (2007).
[17] K. Bartschat, I. Bray, D. V. Fursa, and A. T. Stelbovics, Phys. Rev. A **76**, 024703 (2007).
[18] Computer code SIMION (Scientific Instrument Services, 1027 Old York Road, Rigoes, NJ 08551).
[19] M. S. Pindzola *et al.*, J. Phys. B **40**, R39 (2007).
[20] A. L. Harris, M. Foster, C. Ryan-Anderson, J. L. Peacher, and D. H. Madison, J. Phys. B **41**, 135203 (2008).
[21] S. Jones and D. H. Madison, J. Phys. B **27**, 1423 (1994).
[22] S. Jones and D. H. Madison, Phys. Rev. A **62**, 042701 (2000).
[23] J. F. Hart and G. Herzberg, Phys. Rev. **106**, 79 (1957).
[24] M. Dürr, C. Dimopoulou, A. Dorn, B. Najjari, I. Bray, D. V. Fursa, Zhangjin Chen, D. H. Madison, K. Bartschat, and J. Ullrich, J. Phys. B **39**, 4097 (2006).
[25] J. Röder, H. Ehrhardt, I. Bray, and D. V. Fursa, J. Phys. B **30**, 1309 (1997).
[26] D. H. Madison, M. Schulz, S. Jones, M. Foster, R. Moshammer, and J. Ullrich, J. Phys. B **35**, 3297 (2002).